Mitigation of Cross-Beam Energy Transfer in Ignition-Scale Polar-Direct-Drive Target Designs for the National Ignition Facility

In inertial confinement fusion (ICF), a high-powered laser-driven ablation process is used to implode a spherical shell composed largely of fuel [approximately equimolar deuterium (D) and tritium (T)], producing a central volume (the "hot spot") of high density and ion temperature. In the "direct-drive" scheme, the ablation is accomplished by direct illumination of the target using a spherical distribution of short-wavelength ($\lambda \lesssim 351$-nm) UV laser beams. The inertially confined fuel ions rapidly undergo fusion reactions, producing 3.5-MeV alpha particles, some of which are stopped in both the central region and the surrounding dense DT shell. Ignition occurs when these alpha particles deposit enough energy to launch a thermonuclear burn wave, consuming a fraction of the fuel (depending on the imploded fuel's total areal density) before the high pressure generated by the burn wave causes the target to disassemble. Ignition is predicted to occur if the fuel's internal energy exceeds a minimum value,[1]

$$E_{\min} \approx (50.8 \text{ kJ})\, \alpha_{\text{in}}^{1.88} \left(v_{\text{imp}}\big/300 \text{ km/s}\right)^{-5.89}$$

$$\times \left(P/100 \text{ Mbar}\right)^{-0.77}, \tag{1}$$

where α_{in} is the ratio of the pressure to the Fermi-degenerate fuel pressure (the "adiabat") in the dense DT shell, v_{imp} is the peak shell implosion speed, and P is the ablation pressure. The direct-drive approach is of interest because, for the same incident laser energy, it couples ~3 to 5× more energy into the imploding capsule than indirect drive, enabling more fuel mass to be imploded and lowering the threshold on hot-spot energy $E_{\min}$ as well as the pressure and, therefore, convergence. Note that the threshold energy $E_{\min}$ in Eq. (1) depends sensitively on the implosion speed, which in turn is directly related to the energy coupled to the ablating shell.

Ignition and total fusion yield are directly connected to the volume of the hot spot, the central region in which the temperatures and densities are sufficient to initiate fusion reactions. This volume is reduced by perturbations on the inner edge of the shell that are seeded by a number of sources, including laser-drive nonuniformities and target imperfections, and grow as a result of the Rayleigh–Taylor instability as the shell is decelerated by the pressure of the interior gas.[2] As this volume is reduced, so is the energy coupled to the hot spot. Deviations from 1-D implosions can also result in incomplete stagnation, producing residual kinetic energy and reduced hot-spot pressure. In its current configuration, the laser beam ports at the National Ignition Facility (NIF)[3] are preferentially distributed toward the poles of the target chamber, designed primarily for use with x-ray–driven targets enclosed in a hohlraum. Direct-drive implosions using this configuration ["polar direct drive" (PDD)[4,5]] require beam repointing to compensate for the lack of equatorial beams and higher incident angles in the equatorial region.

In order to credibly design PDD targets, it is critical to incorporate the important physics in the simulations. Laser direct-drive experiments on OMEGA[6] and the NIF[7–9] have demonstrated that it is necessary to model both cross-beam energy transfer (CBET) and nonlocal electron heat transport. CBET is seeded stimulated Brillouin scattering (SBS) in which two beams interact by means of an intermediate ion-acoustic wave,[10] increasing the scattered light, reducing the ablation pressure, and decreasing energy coupling and shell velocity (especially in the equatorial region for PDD targets). Nonlocal electrons in the corona, by contrast, increase the conversion efficiency of laser energy to shell kinetic energy by means of their larger mean free paths and more-effective transport. These effects have been observed to be important in the modeling of numerous implosion experiments at comparable laser intensities on OMEGA.[11,12] While nonlocal electron transport can increase the hydrodynamic efficiency of the implosion, CBET scatters a sizable fraction (~20% to 30%) of the incident laser energy, reducing both P and v_{imp} and raising $E_{\min}$. The magnitude of these combined effects is illustrated in Fig. 152.6, where the ablation pressure and shell speed are shown as a function of wavelength-detuning separation, $\Delta\lambda$. The $\Delta\lambda = 0$ limit indicates the effects of unmitigated CBET, compared with the much higher drive pressure and shell speed that can be achieved when CBET is mitigated by means of wavelength detuning, as described below.
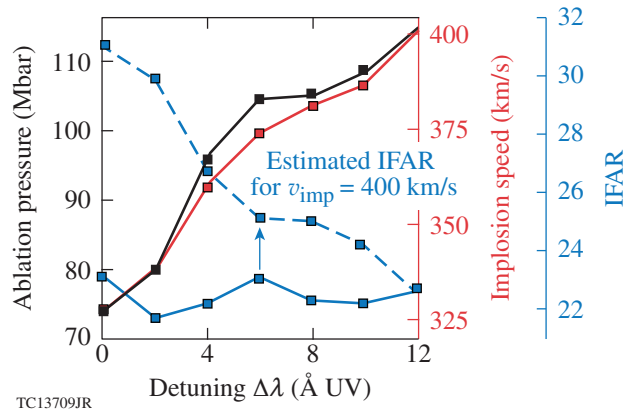
TC13709JR

Figure 152.6

The ablation pressure and implosion speed are shown for the ignition design as functions of wavelength-detuning separation. Also shown (dashed line) is the approximate in-flight aspect ratio (IFAR) expected for a shell with mass reduced by the amount needed to recover the original 400-km/s implosion speed.

The two PDD designs presented in this article—the alpha-burning design and the lower-adiabat ignition design—address the twin constraints of sufficient shell kinetic energy and implosion uniformity. These are the first ignition-scale direct-drive designs of any dimensionality to include the effects of nonlocal heat transport and CBET. Previous ignition designs did not incorporate this important physics and modeled these processes in an approximate way by using an *ad hoc* flux limiter applied to the classical expression for heat conduction.[13] In these designs, the loss of drive related to CBET is mitigated by detuning the laser-beam wavelengths relative to one another.[14,15] As with previous PDD designs for the NIF, the drive asymmetries caused by the disposition of the beams are controlled through a combination of independent pulse shapes for different groups of beams, tailored laser beam spot shapes, and beam repointing. The alpha burner has a shell adiabat of almost 5 for greater hydrodynamic stability. In a simulation that models only drive perturbations caused by beam geometry, the alpha burner is predicted to generate bootstrap heating with a yield enhancement of 5× by means of alpha deposition, producing over 10^{17} fusion neutrons. The lower-adiabat ignition design (~3) achieves a gain close to 30.

PDD designs have seen vast improvement since the original concept was first proposed by Skupsky *et al*.[4] While that earlier design was not capable of ignition, it included components that have been used in most other laser PDD designs: use of different pulse shapes for different laser beams, repointing of beams toward the equatorial region of the target, and equatorial spot shapes that concentrate energy toward the equator. Each of these components compensates for the reduction in equatorial

ablative drive because of the greater angles of incidence and resulting energy deposition at lower densities for the laser light driving that region. Marozas *et al*.[5] presented the first igniting PDD design. Their design improved on the earlier design by using an automated tuning process for the pulse shape designs. Reference 5 also presented a general process for tuning PDD designs and demonstrated the importance of the time dependence of the relative beam-group energies. Their design also made use of spot shapes apertured by a high-order super-Gaussian envelope, reducing the amount of energy flowing around the target [spot-masking apodization (SMA)[5,16]]. The first design to use a shell of DT ice with a CH ablator rather than a foam/DT shell was that of Collins *et al*.[17] It also applied the previously introduced beam conditioning through smoothing by spectral dispersion (SSD),[18] employing multiple-frequency modulators[19] applied selectively prior to the main "drive" portion of the laser pulse.[20] The more-recent designs of Lafon *et al*.[21] use ablators composed of mid-*Z* elements to reduce perturbation growth resulting from laser imprint by increasing the size of the conduction zones between the laser absorption and ablation regions. PDD designs have also been developed for the shock-ignition scheme,[22] in which a high-intensity laser spike at the end of the drive pulse drives a strong shock, thereby initiating ignition.[23,24] These designs do not include any mechanism for mitigating CBET, nor do they model nonlocal electron heat transport; the work presented in this article includes the first such designs. Finally, an intermediate-energy PDD detuning design for CBET mitigation has been fielded for the first time on the NIF, demonstrating the effectiveness of this approach and exploring the physical mechanism of wavelength detuning.[15] Observables such as the shapes and trajectories of the in-flight shell inferred through radiographs are well modeled with the CBET model described below. These validated models are used in the designs presented in this work.

The consistent result of each of these investigations is that the low equatorial drive can be successfully compensated for in a number of ways. The design of Collins *et al*.[17] is the basis of the designs described here, which employs equatorial pulses with 50%-higher power (within the NIF laser performance envelope) than the polar beams, repoints beams toward the equator, and uses SMA to offset the loss of equatorial drive caused by PDD.

For direct-drive targets of sufficient density scale length and laser intensity, the SBS process responsible for CBET is dynamically important. As mentioned above, this process entails the parametric coupling of incident light with an ion-acoustic wave and a backscattered electromagnetic wave. The efficiency

of energy transfer is determined by a resonance function of the parameter $\eta = \left[(\omega_{pump} - \omega_{probe}) - \mathbf{k}_a \cdot \mathbf{v}\right]/(c_a k_a)$, where ω_{pump} and ω_{probe} are the ray frequencies of the beams losing and gaining energy, respectively; c_a is the outflow sound speed; $\mathbf{k}_a = \mathbf{k}_{pump} - \mathbf{k}_{probe}$ is the ion-acoustic wave vector; and $\mathbf{v}$ is the outflow plasma velocity. Energy transfer from the incoming ray to the outgoing ray occurs as $\eta > 0$ is satisfied in backscatter mode under normal circumstances.[15] CBET is well known in indirect-drive ICF experiments on the NIF, where it has been used to transfer energy between cones of beams to affect low-mode capsule symmetry by means of wavelength detuning,[25] but this forward-scatter mode is unimportant for direct drive.[15] In direct-drive ICF, CBET backscatter typically occurs when an outbound ray is refracted into the path of the central, high-energy region of an inbound beam and the ion-acoustic phase-matching conditions are near resonance. The energy transferred between beams by CBET over a distance ds attenuates the incident laser light by $1 - e^{-d\tau}$, where $d\tau_{CBET} \propto \zeta_{pol} P(\eta) I_{pump} ds$, the resonance function is given by $P(\eta) = \eta \cdot v_a / \left[(\eta v_a)^2 + (1 - \eta^2)^2\right]$, and I_{pump} is the intensity of the "pump" beam. Reduction in energy transfer caused by mismatched inbound–outbound polarization is represented by the factor ζ_{pol}.

CBET is particularly effective at scattering energy from incoming rays and significantly reducing ablation pressure because the matching condition can be met over a large volume, where $|\eta| \approx 1$ and the resonance function $P(\eta)$ peaks. Consider this region in the absence of wavelength detuning: the shift in a ray's frequency resulting from the changing plasma refractive index n_r is small enough that $\omega_{pump} \approx \omega_{probe}$ (Ref. 26). The mass flow in the corona is nearly radial, so CBET backscatter is greatest in a region where $M\mathbf{k}_a \cdot \mathbf{r} \equiv M\cos\theta_a \approx 1$ (where M is the flow Mach number and θ_a is the angle between $\mathbf{k}_a$ and $\mathbf{r}$). This region is largely exterior to the Mach-1 surface where, as M increases radially outward, θ_a decreases so the product is still approximately unity. As a result of the beam angles in the PDD configuration and the lack of usable equatorial beam ports, this resonance region occurs preferentially over the equator where repointed beams from each hemisphere overlap. The CBET power density during the drive pulse for the ignition design, but without detuning, is plotted in Fig. 152.7(a). Note that the CBET power density includes the transferred power resulting from both sidescatter between incoming rays, which has little effect on the target drive, and backscatter between inbound and outbound rays, which is of primary interest here.

The target designs presented here were simulated using the 2-D radiation hydrocode *DRACO*.[27] *DRACO* uses a 3-D ray-based inverse bremsstrahlung energy deposition model
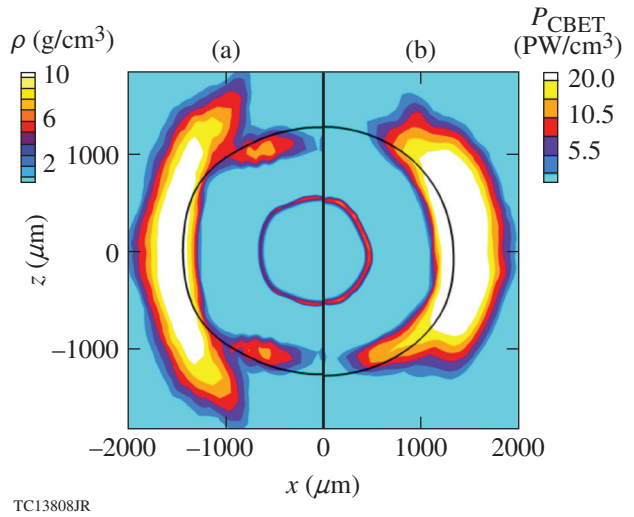

Figure 152.7
The CBET (cross-beam energy transfer) power density during the drive pulse for simulation of the ignition design (a) without wavelength detuning for CBET mitigation and (b) with hemispheric wavelength detuning. With hemispherical detuning, the interaction volume is reduced in extent in the polar angle. The CBET power density includes both backscatter and sidescatter, which accounts for the higher level of power density in (b). The shell mass density is also indicated (with a radius ~500 to 600 μm), showing the greater convergence with wavelength detuning (right). The Mach-1 surface is indicated by the solid black circle.

(*Mazinisin*).[5] The CBET model in *DRACO*, *Adaawam*,[15] uses an angular-spectrum representation (ASR) in which the ASR captures, for each computational zone, the accumulated intensity as a function of direction and color from all the beams that enter that cell, representing the field of pump rays. A pump ray traversing a cell interacts with the other rays, which cross the zones by means of the ASR, using the formalism above. A proportional-integral-differential (PID) predictor–corrector controller iterates until a self-consistent, energy-conserving solution is found. Since the ray-trace approach used in *DRACO* does not presently include the polarization state of the light, random polarization is included by setting $\zeta_{pol} = (1/4)\left[1 + (\hat{\mathbf{k}}_{pump} \cdot \hat{\mathbf{k}}_{probe})^2\right]$ (Ref. 28). This model for CBET has been shown to accurately predict the large-scale morphology of implosions on the NIF when a constant multiplier of 1.5 is applied to $d\tau_{CBET}$ (Refs. 9 and 15). Since experiments have yet to probe plasma conditions (density scale lengths, flow speeds, and electron temperature) relevant to NIF PDD ignition, the equations above for the attenuation caused by CBET are used here without an *ad hoc* multiplier. Using a 1.5 multiplier would reduce the shell speed and require a redesign of the target and likely a reduction in shell mass and corresponding increase in the IFAR. Simulations indicate it is also possible to compensate for an increase in CBET multiplier

by increasing drive power, even though peak drive power is limited by optics damage considerations.

DRACO uses the implicit Schurtz–Nicolaï–Busquet (iSNB) nonlocal heat-transport model,[29] based on the Schurtz–Nicolaï–Busquet (SNB) model.[30] The SNB model computes the nonlocal heat flux using multigroup diffusion by means of a multidimensional convolution integral, which has the effect of delocalizing the Spitzer–Härm heat flux. The iSNB model improves on SNB by solving the diffusion equations implicitly for improved robustness and numerical accuracy. Because of sensitivity in direct-drive ignition to fast-electron preheat, modified mean free paths are used to bring results closer to predictions by more complex but computationally expensive nonlocal models (e.g., Ref. 11). These mean free paths are such that nonlocal electron thermal transport overwhelmingly affects the drive rather than the fuel adiabat. The iSNB model has demonstrated predictive capability for shock timing[29] and shell shape[31] in numerous experiments on OMEGA.

In the wavelength-detuning approach to CBET mitigation, the laser cavities are detuned slightly for different collections of beams to increase the frequency separation, which in turn alters the region over which the CBET efficiency is greatest. The detuning magnitude considered here for the designs presented here is $\Delta\lambda\pm12$ Å (UV). Extension of these results to ±6 Å is discussed below. The designs presented here will require modifications to the NIF, including the ability to extend the wavelength tunability of the laser drive and enhanced beam conditioning such as multifrequency-modulated SSD and distributed polarization rotators. Future target designs that mitigate laser beam imprint may reduce or alter the requirements for enhanced beam smoothing. A cryogenic handling system that reduces the time between when the target is extracted from the cryostat and the start of the laser pulse will also be necessary. It should also be recognized that PDD would also enable the use of external magnetic fields that may enhance fusion performance by reducing thermal conduction losses from the hot spot and more efficiently trapping the alpha particles.[32]

If the outgoing probe rays are detuned to shorter wavelengths (blue-shifted) relative to the pump field, the resonance region moves to greater Mach numbers and correspondingly larger radii, where the beam overlap and corresponding energy transfer are reduced.[15] If the probe rays are red-shifted relative to the pump field, the resonance region moves radially inward, reducing the overlap between the resonance region and the region reached by the rays. Figure 152.7(b) shows the CBET power density for the ignition design but with the simpler

hemispheric wavelength-detuning configuration. Over time, for red-detuned outgoing rays, this resonance region is exposed,[15] reducing the CBET mitigation.

The effectiveness of this approach depends on the choice of which beam groups to "detune" and by how much. Several detuning configurations were investigated (see Fig. 152.8). The
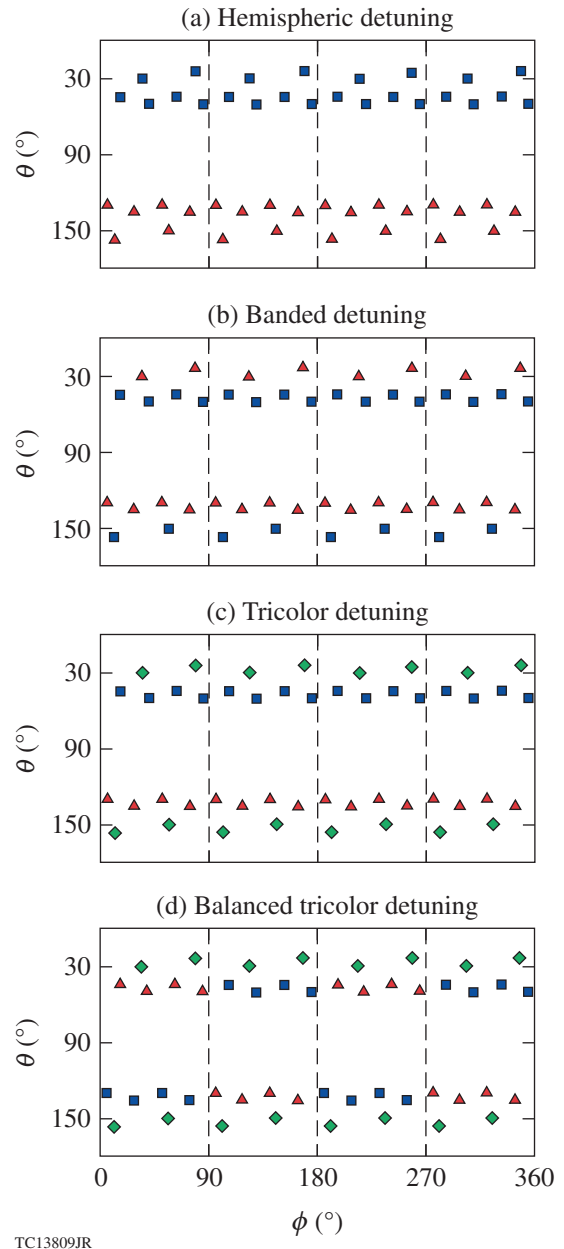

TC13809JR

Figure 152.8
Four of the wavelength-detuning configurations explored in this study. The wavelength shift of each port is indicated by the color of the symbols (where green corresponds to a zero wavelength shift).

laser-absorption efficiency for four of these configurations is shown in Fig. 152.9. Per Fig. 152.8, the hemispheric scheme detunes the beams by hemisphere.[14] This scheme greatly reduces the energy loss caused by the beams interacting across the equator, which is where the greatest scattering occurs, but does not reduce losses caused by interactions between beams from the same hemisphere. The beams on the NIF are divided into four cones for each hemisphere: two inner cones nearer the pole and two outer cones nearer the equator. The banded scheme reverses the sign of the detuning for the two inner cones of beams in each hemisphere, thereby increasing the coupling.
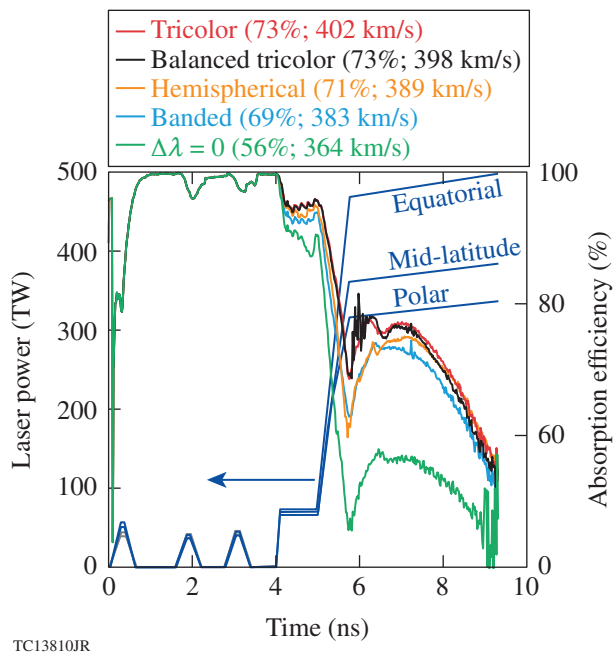

Figure 152.9

Absorption efficiency is shown as a function of time for four detuning configurations for the polar-direct-drive ignition design, modeled by including the effects of CBET and nonlocal electron thermal transport. The case without detuning is also shown. The legend shows the cumulative absorption efficiency as well as the peak implosion speed. Shown in blue are the pulse shapes used in the inner-cone beams (which preferentially illuminate the polar and mid-latitude regions on the target) and the outer-cone (equatorial) beams for the ignition (blue) and alpha-burning (gray, visible only at ~400 ps) designs.

The tricolor configuration improves on both of these by not detuning the inner cones. The tricolor scheme is more effective than the banded scheme because the inner cones interact with both the equatorial beams in the same hemisphere and with the equatorial beams in the opposite hemisphere; by not detuning the inner cones, more energy is regained from the interaction across the equator than is lost to the intrahemispherical interaction. Figure 152.9 also shows the primary effect of nonlocal

heat transport: an increase in absorption efficiency, which occurs especially near the equator where the radial thermal gradient is greater. A comparison between the implosions with and without nonlocal heat transport, shows an increase of ~30% in the absorbed laser energy for the tricolor scheme, resulting in a much higher implosion speed. All three of these schemes introduce a north–south asymmetry, as described above. This asymmetry is greatly reduced by using a fourth configuration, balanced tricolor, in which the tricolor scheme is inverted, north to south, in alternating quadrants.[33,34]

The two designs shown here use a 194-μm DT shell with a 36-μm CH ablator and an outer radius of 1482 μm. Each design uses a triple-picket pulse shape to shape the adiabat.[35] The incident laser energy is 1.8 MJ. Both designs achieve a high implosion speed of ~400 μm/ns, sufficient to generate burn-averaged hot-spot pressures of 190 Gbar for the ignition design and 215 Gbar for the alpha burner, which is higher because of the delayed disassembly. It is important to recognize that x-ray–driven implosions on the NIF have achieved inferred hot-spot pressures well in excess of those calculated in these designs.[36] Both designs have moderately low in-flight aspect ratios (IFAR's), given by the maximum ratio during the implosion of the shell radius to its thickness. The IFAR is an indicator of shell stability, with lower values being less unstable.[37] The ignition design has an IFAR of 23 and a minimum end-of-pulse, density-weighted adiabat of 2.8, and the alpha burner has a somewhat lower IFAR of 21 with a larger ablator adiabat, resulting in an end-of-pulse, density-weighted adiabat of 4.8. Both of these IFAR's are lower than that of their flux-limited predecessor,[17] which also used a CH ablator and was calculated to withstand the effects of laser imprint. (The simulations presented here include only nonuniformities related to port geometry, repointing, CBET, and nonlocal heat transport; sensitivity to other illumination nonuniformities, such as beam power imbalance, and to target imperfections will be investigated in the near future.) The higher fuel adiabat of the alpha burner is reflected in a lower hot-spot convergence fuel ratio of 25, compared to 28 for the ignition design, and a lower peak total fuel areal density of 1.4 g/cm^2, compared to 1.7 g/cm^2 for the ignition design. The ion temperature and density of these designs are shown around the time of peak convergence in Fig. 152.10. The alpha burner achieves a total neutron yield of 1.2×10^{17} (~320 kJ of fusion energy) and the ignition design achieves a yield of 1.8×10^{19}, with 1.8 MJ of incident energy, for a gain of 27. While the alpha burner does not ignite, it operates at a moderate adiabat for acceleration-phase stability, and the neutrons generated by bootstrap heating are over 5× that generated by compression alone. Since this design

lacks an "ignition cliff," it is also less sensitive to drive and target nonuniformities, making this design an ideal platform for initial study; initial estimates suggest the neutron yield for the alpha burner varies approximately linearly with the implosion speed, rather than the much-steeper dependence of an ignition design.

The use of a $\Delta\lambda = \pm12$ Å (UV) detuning bandwidth would require significant modifications to the NIF laser chain as presently understood. It may be possible, however, to obtain ignition-relevant hot-spot conditions for lower values of $\Delta\lambda$. Figure 152.6 shows, for the ignition design, the dependence of ablation pressure and implosion speed on $\Delta\lambda$. (The pointing and detuning configurations are held constant.) The volume over which CBET is active changes as $\Delta\lambda$ is varied; this is the most likely cause of the second-order nonlinearities in the dependence on $\Delta\lambda$. This plot makes clear the effectiveness of detuning as a mitigation scheme; detuning by ±12 Å increases the drive pressure by over 50% and the implosion speed by ~10%. As expected, the CBET efficiency increases as $\Delta\lambda$ decreases, reducing the coupling and raising E_{min}. This reduction in coupling may, in principle, be offset by a reduction in fuel mass at the cost of increased IFAR. Figure 152.6 also shows the IFAR that would result from reducing the fuel mass in order to obtain the original shell speed of 400 km/s. Reducing $\Delta\lambda$ to ±6 Å corresponds to an increase in the IFAR from 23 to 25 and may require greater beam smoothing to achieve ignition. However, the alpha burner is already on a high shell adiabat and is less sensitive to imprint. Development of a PDD alpha burner with a thinner shell and $\Delta\lambda = \pm6$ Å is a natural next step.

The two designs presented here—the first of their kind—demonstrate a promising approach to generating high-energy densities on the NIF and offer a useful research platform for ICF ignition. These designs have peak equatorial intensities of $\sim1.4 \times 10^{15}$ W/cm^2 and are likely to experience some degree of fast-electron preheat because of two-plasmon decay and stimulated Raman scattering. A solution for this preheat has already been proposed and will be explored, in which the ablator is doped with mid-Z elements, in order to raise the electron temperature and the instability threshold and increase absorption efficiency.[9,21,38] This is likely to be far less of a design issue for the alpha burner, which already operates on a high adiabat. This is, in part, because of the lack of the ignition cliff mentioned above. It is also true because an increase of $\Delta\alpha = 1$ (where α is the adiabat) is a $\delta\ln\alpha = 50\%$ increase for an $\alpha = 2$ ignition design but only a $\delta\ln\alpha = 20\%$ increase for an $\alpha = 5$ alpha burner, and the factional increase in hot-spot pressure (in the absence of alpha heating, which is relevant for achieving ignition-scale conditions needed for both target designs) is $\delta\ln p_{hs} \approx -0.9\,\delta\ln\alpha$ (Ref. 22), where p_{hs} is the hot-spot pressure. Furthermore, the designs presented here are modeled in 2-D, although nonaxisymmetric perturbations are expected from both the laser-port geometry (which introduces a perturbation with azimuthal mode number $m = 4$) and the detuning configuration ($m = 2$). While these low modes may be compensated by using azimuthal target "shimming,"[39,40] other detuning configurations that do not introduce nonaxisymmetric modes are also being developed. As mentioned above, an embedded external magnetic field may also improve the target performance.
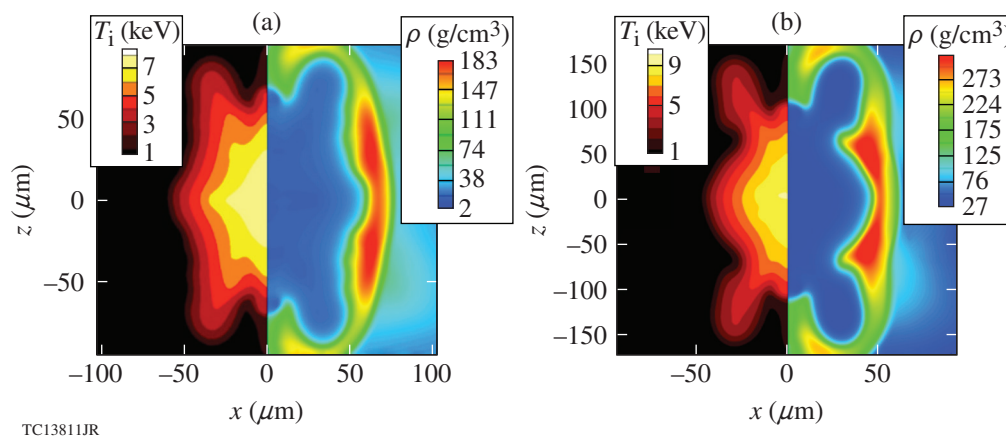

Figure 152.10

(a) The alpha-burning and (b) ignition designs are shown near peak compression. On the left of each contour plot is the ion temperature and on the right is the mass density.

REFERENCES

1. M. C. Herrmann, M. Tabak, and J. D. Lindl, Nucl. Fusion **41**, 99 (2001).

2. E. M. Campbell, V. N. Goncharov, T. C. Sangster, S. P. Regan, P. B. Radha, R. Betti, J. F. Myatt, D. H. Froula, M. J. Rosenberg, I. V. Igumenshchev, W. Seka, A. A. Solodov, A. V. Maximov, J. A. Marozas, T. J. B. Collins, D. Turnbull, F. J. Marshall, A. Shvydky, J. P. Knauer, R. L. McCrory, A. B. Sefkow, M. Hohenberger, P. A. Michel, T. Chapman, L. Masse, C. Goyon, S. Ross, J. W. Bates, M. Karasik, J. Oh, J. Weaver, A. J. Schmitt, K. Obenschain, S. P. Obenschain, S. Reyes, and B. Van Wonterghem, Matter and Radiation at Extremes **2**, 37 (2017).

3. E. M. Campbell and W. J. Hogan, Plasma Phys. Control. Fusion **41**, B39 (1999).

4. S. Skupsky, J. A. Marozas, R. S. Craxton, R. Betti, T. J. B. Collins, J. A. Delettrez, V. N. Goncharov, P. W. McKenty, P. B. Radha, T. R. Boehly, J. P. Knauer, F. J. Marshall, D. R. Harding, J. D. Kilkenny, D. D. Meyerhofer, T. C. Sangster, and R. L. McCrory, Phys. Plasmas **11**, 2763 (2004).

5. J. A. Marozas, F. J. Marshall, R. S. Craxton, I. V. Igumenshchev, S. Skupsky, M. J. Bonino, T. J. B. Collins, R. Epstein, V. Yu. Glebov, D. Jacobs-Perkins, J. P. Knauer, R. L. McCrory, P. W. McKenty, D. D. Meyerhofer, S. G. Noyes, P. B. Radha, T. C. Sangster, W. Seka, and V. A. Smalyuk, Phys. Plasmas **13**, 056311 (2006).

6. V. N. Goncharov, S. P. Regan, E. M. Campbell, T. C. Sangster, P. B. Radha, J. F. Myatt, D. H. Froula, R. Betti, T. R. Boehly, J. A. Delettrez, D. H. Edgell, R. Epstein, C. J. Forrest, V. Yu. Glebov, D. R. Harding, S. X. Hu, I. V. Igumenshchev, F. J. Marshall, R. L. McCrory, D. T. Michel, W. Seka, A. Shvydky, C. Stoeckl, W. Theobald, and M. Gatu-Johnson, Plasma Phys. Control. Fusion **59**, 014008 (2017).

7. T. J. Murphy, N. S. Krasheninnikova, G. A. Kyrala, P. A. Bradley, J. A. Baumgaertel, J. A. Cobble, P. Hakel, S. C. Hsu, J. L. Kline, D. S. Montgomery, K. A. D. Obrey, R. C. Shah, I. L. Tregillis, M. J. Schmitt, R. J. Kanzleiter, S. H. Batha, R. J. Wallace, S. D. Bhandarkar, P. Fitzsimmons, M. L. Hoppe, A. Nikroo, M. Hohenberger, P. W. McKenty, H. G. Rinderknecht, M. J. Rosenberg, and R. D. Petrasso, Phys. Plasmas **22**, 092707 (2015).

8. M. Hohenberger, P. B. Radha, J. F. Myatt, S. LePape, J. A. Marozas, F. J. Marshall, D. T. Michel, S. P. Regan, W. Seka, A. Shvydky, T. C. Sangster, J. W. Bates, R. Betti, T. R. Boehly, M. J. Bonino, D. T. Casey, T. J. B. Collins, R. S. Craxton, J. A. Delettrez, D. H. Edgell, R. Epstein, G. Fiksel, P. Fitzsimmons, J. A. Frenje, D. H. Froula, V. N. Goncharov, D. R. Harding, D. H. Kalantar, M. Karasik, T. J. Kessler, J. D. Kilkenny, J. P. Knauer, C. Kurz, M. Lafon, K. N. LaFortune, B. J. MacGowan, A. J. Mackinnon, A. G. MacPhee, R. L. McCrory, P. W. McKenty, J. F. Meeker, D. D. Meyerhofer, S. R. Nagel, A. Nikroo, S. Obenschain, R. D. Petrasso, J. E. Ralph, H. G. Rinderknecht, M. J. Rosenberg, A. J. Schmitt, R. J. Wallace, J. Weaver, C. Widmayer, S. Skupsky, A. A. Solodov, C. Stoeckl, B. Yaakobi, and J. D. Zuegel, Phys. Plasmas **22**, 056308 (2015).

9. P. B. Radha, M. Hohenberger, D. H. Edgell, J. A. Marozas, F. J. Marshall, D. T. Michel, M. J. Rosenberg, W. Seka, A. Shvydky, T. R. Boehly, T. J. B. Collins, E. M. Campbell, R. S. Craxton, J. A. Delettrez, S. N. Dixit, J. A. Frenje, D. H. Froula, V. N. Goncharov, S. X. Hu, J. P. Knauer, R. L. McCrory, P. W. McKenty, D. D. Meyerhofer, J. Moody, J. F. Myatt, R. D. Petrasso, S. P. Regan, T. C. Sangster, H. Sio, S. Skupsky, and A. Zylstra, Phys. Plasmas **23**, 056305 (2016).

10. C. J. Randall, J. R. Albritton, and J. J. Thomson, Phys. Fluids **24**, 1474 (1981).

11. V. N. Goncharov, O. V. Gotchev, E. Vianello, T. R. Boehly, J. P. Knauer, P. W. McKenty, P. B. Radha, S. P. Regan, T. C. Sangster, S. Skupsky, V. A. Smalyuk, R. Betti, R. L. McCrory, D. D. Meyerhofer, and C. Cherfils-Clérouin, Phys. Plasmas **13**, 012702 (2006).

12. V. N. Goncharov, T. C. Sangster, R. Betti, T. R. Boehly, M. J. Bonino, T. J. B. Collins, R. S. Craxton, J. A. Delettrez, D. H. Edgell, R. Epstein, R. K. Follet, C. J. Forrest, D. H. Froula, V. Yu. Glebov, D. R. Harding, R. J. Henchen, S. X. Hu, I. V. Igumenshchev, R. Janezic, J. H. Kelly, T. J. Kessler, T. Z. Kosc, S. J. Loucks, J. A. Marozas, F. J. Marshall, A. V. Maximov, R. L. McCrory, P. W. McKenty, D. D. Meyerhofer, D. T. Michel, J. F. Myatt, R. Nora, P. B. Radha, S. P. Regan, W. Seka, W. T. Shmayda, R. W. Short, A. Shvydky, S. Skupsky, C. Stoeckl, B. Yaakobi, J. A. Frenje, M. Gatu-Johnson, R. D. Petrasso, and D. T. Casey, Phys. Plasmas **21**, 056315 (2014).

13. W. L. Kruer, in *The Physics of Laser Plasma Interactions*, Frontiers in Physics, Vol. 73, edited by D. Pines (Westview, Boulder, CO, 2003).

14. J. A. Marozas, T. J. B. Collins, J. D. Zuegel, P. B. Radha, F. J. Marshall, and W. Seka, presented at the 44th Annual Anomalous Absorption Conference, Estes Park, CO, 8–13 June 2014.

15. J. A. Marozas, M. Hohenberger, M. J. Rosenberg, D. Turnbull, T. J. B. Collins, P. B. Radha, P. W. McKenty, J. D. Zuegel, F. J. Marshall, S. P. Regan, T. C. Sangster, W. Seka, E. M. Campbell, V. N. Goncharov, M. W. Bowers, J.-M. G. DiNicola, G. Erbert, B. J. MacGowan, L. J. Pelz, and S. T. Yang, "First Observation of Cross-Beam Energy Transfer Mitigation for Direct-Drive Inertial Confinement Fusion Implosions Using Wavelength Detuning at the National Ignition Facility," submitted to Physical Review Letters.

16. J. A. Marozas, T. J. B. Collins, J. D. Zuegel, P. W. McKenty, D. Cao, S. Fochs, and P. B. Radha, J. Phys.: Conf. Ser. **717**, 012107 (2016).

17. T. J. B. Collins, J. A. Marozas, K. S. Anderson, R. Betti, R. S. Craxton, J. A. Delettrez, V. N. Goncharov, D. R. Harding, F. J. Marshall, R. L. McCrory, D. D. Meyerhofer, P. W. McKenty, P. B. Radha, A. Shvydky, S. Skupsky, and J. D. Zuegel, Phys. Plasmas **19**, 056308 (2012).

18. S. Skupsky and T. Kessler, Opt. Commun. **70**, 123 (1989).

19. J. A. Marozas, J. D. Zuegel, and T. J. B. Collins, Bull. Am. Phys. Soc. **53**, 249 (2008).

20. P. W. McKenty, J. A. Marozas, V. N. Goncharov, K. S. Anderson, R. Betti, D. D. Meyerhofer, P. B. Radha, T. C. Sangster, S. Skupsky, and R. L. McCrory, Bull. Am. Phys. Soc. **51**, 295 (2006).

21. M. Lafon, R. Betti, K. S. Anderson, T. J. B. Collins, R. Epstein, P. W. McKenty, J. F. Myatt, A. Shvydky, and S. Skupsky, Phys. Plasmas **22**, 032703 (2015).

22. R. Betti, C. D. Zhou, K. S. Anderson, L. J. Perkins, W. Theobald, and A. A. Solodov, Phys. Rev. Lett. **98**, 155001 (2007).

23. K. S. Anderson, R. Betti, P. W. McKenty, T. J. B. Collins, M. Hohenberger, W. Theobald, R. S. Craxton, J. A. Delettrez, M. Lafon, J. A. Marozas, R. Nora, S. Skupsky, and A. Shvydky, Phys. Plasmas **20**, 056312 (2013).

24. M. Temporal *et al.*, High Power Laser Sci. Eng. **2**, e37 (2014).

25. P. Michel *et al.*, Phys. Plasmas **16**, 042702 (2009).

26. T. P. Gill, *The Doppler Effect: An Introduction to the Theory of the Effect* (Logos, London, 1965).

27. P. B. Radha, V. N. Goncharov, T. J. B. Collins, J. A. Delettrez, Y. Elbaz, V. Yu. Glebov, R. L. Keck, D. E. Keller, J. P. Knauer, J. A. Marozas, F. J. Marshall, P. W. McKenty, D. D. Meyerhofer, S. P. Regan, T. C. Sangster, D. Shvarts, S. Skupsky, Y. Srebro, R. P. J. Town, and C. Stoeckl, Phys. Plasmas **12**, 032702 (2005).

28. P. Michel, Lawrence Livermore National Laboratory, private communication (2014).

29. D. Cao, G. Moses, and J. Delettrez, Phys. Plasmas **22**, 082308 (2015).

30. G. P. Schurtz, Ph. D. Nicolaï, and M. Busquet, Phys. Plasmas **7**, 4238 (2000).

31. S. P. Regan, V. N. Goncharov, I. V. Igumenshchev, T. C. Sangster, R. Betti, A. Bose, T. R. Boehly, M. J. Bonino, E. M. Campbell, D. Cao, T. J. B. Collins, R. S. Craxton, A. K. Davis, J. A. Delettrez, D. H. Edgell, R. Epstein, C. J. Forrest, J. A. Frenje, D. H. Froula, M. Gatu Johnson, V. Yu. Glebov, D. R. Harding, M. Hohenberger, S. X. Hu, D. Jacobs-Perkins, R. T. Janezic, M. Karasik, R. L. Keck, J. H. Kelly, T. J. Kessler, J. P. Knauer, T. Z. Kosc, S. J. Loucks, J. A. Marozas, F. J. Marshall, R. L. McCrory, P. W. McKenty, D. D. Meyerhofer, D. T. Michel, J. F. Myatt, S. P. Obenschain, R. D. Petrasso, R. B. Radha, B. Rice, M. Rosenberg, A. J. Schmitt, M. J. Schmitt, W. Seka, W. T. Shmayda, M. J. Shoup III, A. Shvydky, S. Skupsky, A. A. Solodov, C. Stoeckl, W. Theobald, J. Ulreich, M. D. Wittman, K. M. Woo, B. Yaakobi, and J. D. Zuegel, Phys. Rev. Lett. **117**, 025001 (2016); **117**, 059903(E) (2016).

32. L. J. Perkins *et al.*, Phys. Plasmas **20**, 072708 (2013).

33. J. A. Marozas, T. J. B. Collins, P. W. McKenty, and J. D. Zuegel, Bull. Am. Phys. Soc. **60**, 167 (2015).

34. T. J. B. Collins, J. A. Marozas, P. W. McKenty, and S. Skupsky, Bull. Am. Phys. Soc. **60**, 29 (2015).

35. V. N. Goncharov, T. C. Sangster, T. R. Boehly, S. X. Hu, I. V. Igumenshchev, F. J. Marshall, R. L. McCrory, D. D. Meyerhofer, P. B. Radha, W. Seka, S. Skupsky, C. Stoeckl, D. T. Casey, J. A. Frenje, and R. D. Petrasso, Phys. Rev. Lett. **104**, 165001 (2010).

36. R. Betti and O. A. Hurricane, Nat. Phys. **12**, 435 (2016).

37. S. Atzeni and J. Meyer-ter-Vehn, *The Physics of Inertial Fusion: Beam Plasma Interaction, Hydrodynamics, Hot Dense Matter*, 1st ed., International Series of Monographs on Physics, Vol. 125 (Oxford University Press, Oxford, 2004).

38. R. K. Follett, J. A. Delettrez, D. H. Edgell, V. N. Goncharov, R. J. Henchen, J. Katz, D. T. Michel, J. F. Myatt, J. Shaw, A. A. Solodov, C. Stoeckl, B. Yaakobi, and D. H. Froula, Phys. Rev. Lett. **116**, 155002 (2016).

39. S. Skupsky, R. S. Craxton, F. J. Marshall, R. Betti, T. J. B. Collins, R. Epstein, V. N. Goncharov, I. V. Igumenshchev, J. A. Marozas, P. W. McKenty, P. B. Radha, J. D. Kilkenny, D. D. Meyerhofer, T. C. Sangster, and R. L. McCrory, J. Phys. IV France **133**, 233 (2006).

40. D. S. Clark *et al.*, Phys. Plasmas **23**, 072707 (2016).